The Astrophysical Journal, 917:20 (9pp), 2021 August 10 https://doi.org/10.3847/1538-4357/ac0729

Evidence Suggesting That 'Oumuamua Is the ∼30 Myr Old Product of a Molecular Cloud

Cheng-Han Hsieh, Gregory Laughlin, and Héctor G. Arce
Department of Astronomy, Yale University, New Haven, CT 06511, USA; cheng-han.hsieh@yale.edu
Received 2021 February 9; revised 2021 May 27; accepted 2021 May 29; published 2021 August 10

Abstract

The appearance of interstellar objects (ISOs) in the solar system—and specifically the arrival of 1I/'Oumuamua—points to a significant number density of free-floating bodies in the solar neighborhood. We review the details of 'Oumuamua's pre-encounter Galactic orbit, which intersected the solar system at very nearly its maximum vertical and radial excursion relative to the Galactic plane. These kinematic features are strongly emblematic of nearby young stellar associations. We obtain an a priori order-of-magnitude age estimate for 'Oumuamua by comparing its orbit to the orbits of 50,899 F-type stars drawn from Gaia DR2; a diffusion model then suggests a ∼35 Myr dynamical age. We compare 'Oumuamua's orbit with the trajectories of individual nearby moving groups, confirming that its motion is fully consistent with membership in the Carina (CAR) moving group with an age of ∼30 Myr. We conduct Monte Carlo simulations that trace the orbits of test particles ejected from the stars in the CAR association. The simulations indicate that in order to uniformly populate the $\sim 10^6$ pc^3 volume occupied by CAR members with the inferred number density, $n = 0.2$ au^{-3}, of ISOs implied by Pan-STARRS's detection of 'Oumuamua, the required ejection mass is $M \sim 500\ M_{\rm Jup}$ per known star within the CAR association. This suggests that the Pan-STARRS observation is in significant tension with scenarios that posit 'Oumuamua's formation and ejection from a protostellar disk.

Unified Astronomy Thesaurus concepts: Interstellar objects (52); Molecular clouds (1072); Orbits (1184); Comets (280); Asteroids (72); Asteroid dynamics (2210); Milky Way Galaxy (1054)

Supporting material: interactive figures

1. Introduction

The discoveries of the first two interstellar objects (ISOs), 1I/'Oumuamua and 2I/Borisov, provide a study in contrasts. 'Oumuamua displayed a number of startling properties, including a light curve with large variations (Bannister et al. 2017; Jewitt et al. 2017; Knight et al. 2017; Meech et al. 2017; Bolin et al. 2018), a lack of coma or detectable outgassing (Trilling et al. 2018), an anomalous component to its acceleration (Micheli et al. 2018), and an unusual pre-encounter trajectory that placed it nearly exactly at the local standard of rest (Mamajek 2017). The second interstellar object, Borisov, by contrast, has behaved in every respect in the manner expected of comets (Bolin et al. 2020).

'Oumuamua's composition and its point of origin have been the subject of debate from the very moment it was discovered. Its kinematics suggest that it is very young, and a detailed analysis of its trajectory strongly suggests kinship with a local moving group. Hallatt & Wiegert (2020) showed that the Carina and Columba associations provide particularly compelling matches.

The Galactic population of free-floating objects is continually augmented by icy planetesimals that are ejected from protoplanetary disks by close orbital encounters with embedded giant planets. The solar system itself is estimated to have contributed of order $M \sim 30\ M_\oplus$ of planetesimals to interstellar space, largely as a consequence of scattering by Jupiter (Tsiganis et al. 2005; Levison et al. 2008). A process of this type was almost certainly the mechanism behind comet Borisov's presence as a freely orbiting object in the Galactic potential, and it remains a leading hypothesis for 'Oumuamua's origin, although, as we argue here, this interpretation poses difficulties.

Water ice is a dominant constituent of solar system comets, but, as noted by Sekanina (2019), water's large enthalpy of sublimation precludes it from generating 'Oumuamua's observed acceleration. Moreover, the simultaneous lack of coma and presence of nongravitational acceleration have not been observed among comets. 'Oumuamua's shape, which was shown with ∼90% confidence by Mashchenko (2019) to resemble an oblate (6:6:1) spheroid, does not resemble the aspect ratio of known solar system bodies. Moreover, comets are expected to persist indefinitely in the Galactic environment, and so it is surprising that the first-detected ISO had kinematics associated with an extremely young age.

Füglistaler & Pfenniger (2018) raised the possibility that 'Oumuamua could be composed of H_2 ice. This hypothesis was further developed by Seligman & Laughlin (2020), who showed that solid hydrogen can plausibly explain 'Oumuamua's unusual properties. First, with its low enthalpy of sublimation ($S \sim 1$ kJ mol^{-1}), exposed H_2 ice need only cover several percent of 'Oumuamua's surface in order to produce the observed acceleration. Any outgassed flux of molecular H_2 would have eluded detection. H_2 ice has a limited lifetime in the Galactic environment, and Hoang & Loeb (2020) show that a pure H_2-ice object with the current size of 'Oumuamua will last of order $\tau \sim 10$ Myr. The transient nature of H_2 ice thus naturally accounts for 'Oumuamua's exceedingly young kinematics, as well as the strange shape. As pointed out by Domokos et al. (2017), an object that experiences uniform mass loss from its entire surface will develop a large axis ratio prior to disappearing completely. We stress that the formation of objects whose primary initial component is H_2 ice *has not been observed*, although a literature exists that explores how such objects might form in the cold, dense cores of giant

molecular clouds (GMCs; see, e.g., White 1996). A recent study by Levine & Laughlin (2021) finds that the requirement of extremely low temperatures presents the primary apparent bottleneck to present-day formation of ISOs with a significant solid-H_2 component.

The plan for this paper is as follows. In Section 2 we use 'Oumuamua's observed trajectory in conjunction with a recent model of the Galactic potential to review the properties of 'Oumuamua's pre-encounter orbit in the Galaxy. Our dynamical integrations highlight the curious fact that when 'Oumuamua was intercepted, it was very close to the upper limits of both its radial and vertical motions in the Galactic disk. In Section 3 we compare 'Oumuamua's pre-encounter kinematics with the motions of nearby young associations. This exercise illustrates the apparent connection to the Carina and Columba young associations that was discovered by Hallatt & Wiegert (2020). In particular, orbital integration of 'Oumuamua demonstrates full consistency with membership in the Carina association. In Section 4 we use Monte Carlo simulations to demonstrate that, given the relatively small number of stars associated with the Carina moving groups, it is highly unlikely that an object ejected from a disk surrounding one of the Carina stars would appear within the search volume probed by Pan-STARRS. 'Oumuamua's appearance suggests that the GMC that gave rise to the Carina association produced a large quantity of short-lived objects, but even this interpretation is problematic given the vast number of such objects that are inferred.

2. 'Oumuamua's Pre-encounter Orbit

We use the Rebound (Rein & Liu 2012) integration package's high-precision IAS15 scheme (Rein & Spiegel 2015) to model 'Oumuamua's solar system trajectory, as well as Borisov's trajectory for comparison. We adopted ephemerides from NASA's JPL HORIZONS database,[1] and we modeled gravitational forces from the Sun and planets in the solar system (Rein & Spiegel 2015). Nongravitational forces, which amounted to $a \sim 0.001\, g_{\odot} \hat{r}$ for 'Oumuamua during the 2-month interval in which it was observed (Micheli et al. 2018), were not included.

We first integrated backward to determine the distance and velocity of the two objects with respect to the Sun a century ago (specifically, we back-traced to 1919 December 25). At that moment, 'Oumuamua was moving at a near-constant heliocentric velocity of 26.47 km s^{-1} and was at a heliocentric distance of 551.63 au, whereas Borisov had a heliocentric velocity of 32.33 km s^{-1} and a heliocentric distance of 685.39 au.

We used HORIZONS to calculate the average change in R. A. and decl. for 'Oumuamua and Borisov over a 10 yr time interval spanning 1919 through 1929, giving the objects' pre-encounter proper motions in the plane of sky with respect to the Sun. Combining the proper motions with the known speeds relative to the Sun, we obtained the pre-encounter heliocentric radial velocities. This information is needed for calculating Galactocentric orbits.

To simulate the orbits within the Milky Way, we first converted the International Celestial Reference System coordinates employed in the solar system trajectory calculations to the Galactic coordinate system. The velocity of the Sun in Galactic coordinates (Schönrich et al. 2010)[2] is $(U_{\odot} = 11.1, V_{\odot} = 232.24, W_{\odot} = 7.25)$ km s^{-1}, and the vertical position of the Sun is $z = 27.0$ pc above the Galactic disk midplane. In this system, in 1919, 'Oumuamua was located at (X, Y, $Z = -8299.95490805$, 0.00226655, 27.0007947) pc relative to the Galactic center and was moving with a Galactic velocity of $(U_O = -0.522, V_O = 209.779, W_O = -0.574)$ km s^{-1}.[3] Its relative velocity with respect to the Sun was $(U = -11.622, V = -22.461, W = -7.824)$ km s^{-1}, in good agreement with the heliocentric velocity $(U = -11.457, V = -22.395, W = -7.746)$ km s^{-1} previously reported by Mamajek (2017).

Similarly, in 1919, Borisov was located at (X, Y, $Z = -8299.95835444$, 0.00242457, 26.99990599) pc relative to the Galactic center and was moving with a Galactic velocity of $(U_O = 33.005, V_O = 208.486, W_O = 8.286)$ km s^{-1}, giving a relative velocity with respect to the Sun of $(U = 21.905, V = -23.754, W = 1.036)$ km s^{-1}. When combined with the solar system's Galactocentric position, these velocities permit the bodies' trajectories in the Galactic potential to be examined.

We use Gala (Price-Whelan 2017), an Astropy-affiliated package, to simulate the Galactic orbits of the ISOs. We employ a model of the Milky Way potential that consists of a bulge and nucleus (Hernquist 1990), a disk (Miyamoto & Nagai 1975), and a Navarro–Frenk–White halo (Navarro et al. 1997). These structural parameters were chosen for consistency with Bovy (2015). We used a high-order Dormand–Prince 85(3) integration scheme (Dormand & Prince 1980) to trace the orbits of 'Oumuamua, Borisov, and 796,757 known solar neighborhood stars for 500 Myr into the past. All of the bodies were followed with a time-step resolution of 1 Myr.

The simulated orbits (in the x–y plane and in the ρ–z plane) for 'Oumuamua, Borisov, and the Sun are shown in Figure 1, which emphasizes a striking feature of 'Oumuamua's orbit. It encountered the Sun at a moment where it was close to simultaneously experiencing both its maximum radial and vertical excursions. At the moment of encounter, it had $z \sim 27$ pc and its current normalized radial position was $(R_0 - R_{\rm min})/\Delta R = 0.965$), where R_0 is the current position, $R_{\rm min}$ is the minimum radial excursion from the Galactic center, and the ΔR is the radial excursion range. Our integration indicates that 'Oumuamua spends less than ~2% of its time with $z \geqslant 27$ pc and $(R_0 - R_{\rm min})/\Delta R > 0.965$. This coincidence would generally be unexpected for a first detection and suggests that 'Oumuamua belongs to a short-lived population.

3. 'Oumuamua's Age and Point of Origin

The orbits of interstellar objects correlate with age. For the specific case of 'Oumuamua, Almeida-Fernandes & Rocha-Pinto (2018) investigated how the orbital eccentricity, e, the maximum excursion from the Galactic plane, $z_{\rm max}$, the perigalactic radius, $R_{\rm min}$, and the apogalactic radius, $R_{\rm max}$, of stars evolve with time, and they used these relations to derive a kinematic age for 'Oumuamua of $\tau_O \sim 0.5$ Gyr, indicating that the ISO is quite young in comparison to the Galaxy.

[1] https://ssd.jpl.nasa.gov/horizons.cgi

[2] As implemented in https://docs.astropy.org/en/stable/coordinates/.

[3] Note that we did not keep track of the uncertainties for the X, Y, Z, U, V, W coordinates of 'Oumuamua and Borisov in 1919. The Rebound simulated orbits at solar system scale have extremely small uncertainty as compared to the Galactic simulations by Gala. The uncertainty is also well within the uncertainty of the Sun's X, Y, Z, U, V, W inside the Milky Way.

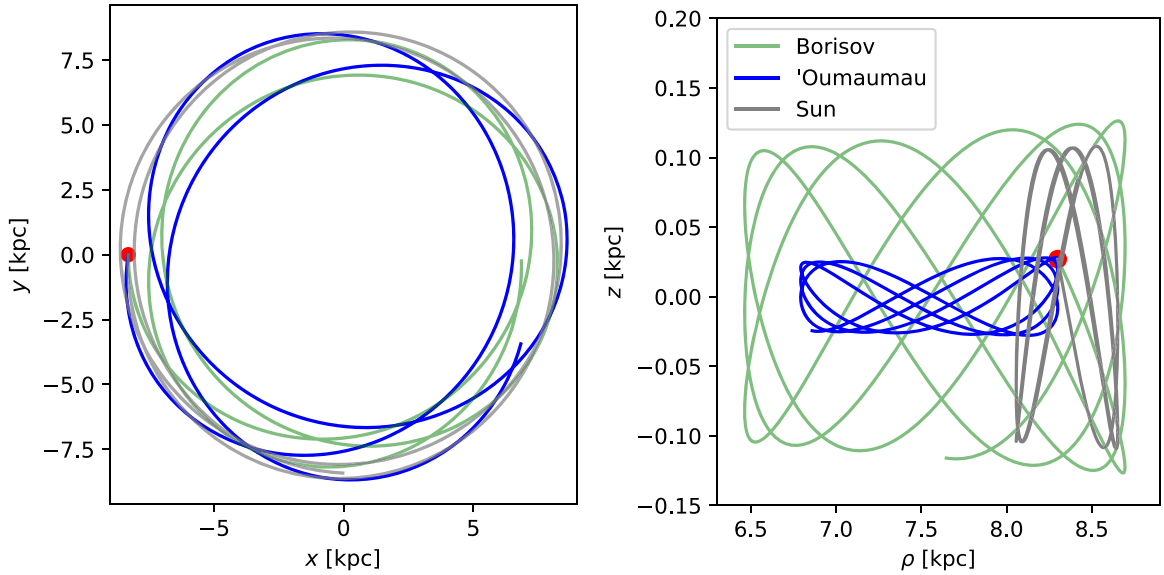

Figure 1. 'Oumuamua's and Borisov's Galactic orbit integrated for 500 Myr into the past. The left panel is in Cartesian coordinates, and the right panel is in cylindrical coordinates, with ρ representing the radial distance from the Galactic center. The red circle marks the current position of the Sun.

The age estimate of Almeida-Fernandes & Rocha-Pinto (2018) draws on the correlation between the Galactic orbital parameters and the isochrone ages of 14,139 stars in the Geneva–Copenhagen Survey (GCS; Nordström et al. 2004). In the GCS, however, more than 90% of the sample stars are older than 1 Gyr, so the statistics are sparse for characterizing the generic orbital properties of the youngest stars. The phase-space distribution function for ISOs of size $D \geqslant 100$ m, by comparison, is quadrillions of times more finely grained than that of stars, and this contrast motivates an independent estimate of 'Oumuamua's (and Borisov's) age.

We do this by comparing the orbits of the interstellar objects to the orbits of high-mass and low-mass stars in the solar vicinity. High-mass stars persist for a few Gyr, while many low-mass stars do not evolve significantly in a Hubble time. On average, the vertical dispersion increases with age, permitting a kinematic age estimate for an ISO with a known orbit.

We first select the 796,757 stars from the DR2 catalog (Gaia Collaboration et al. 2018) having $d < 300$ pc, along with complete radial velocity and proper-motion information. Proceeding from the color–magnitude diagram of these stars, we apply the following criteria to separate high-mass stars (typically F-type stars) and low-mass stars (typically K- and M-type dwarfs):

$$\text{HM: } 0.5 < G_{\rm BP} - G_{\rm RP} < 0.7 \quad (1)$$

$$2 < M_G < 3.75 \quad (2)$$

$$\text{LM: } 2.0 < G_{\rm BP} - G_{\rm RP} < 2.6 \quad (3)$$

$$8.2 < M_G < 10.4, \quad (4)$$

where $G_{\rm BP}$ and $G_{\rm RP}$ are the Gaia bands covering 330–680 nm and 630–1050 nm in wavelength, respectively. The two groups are shown in Figure 2. We restrict the analysis to stars located within 200 pc of the midplane to prevent biasing the sample toward high-mass stars as a consequence of their intrinsic luminosities. This cutoff falls within the $z \sim 300$ pc stellar disk scale height (Kent et al. 1991; López-Corredoira et al. 2002; McMillan 2011).

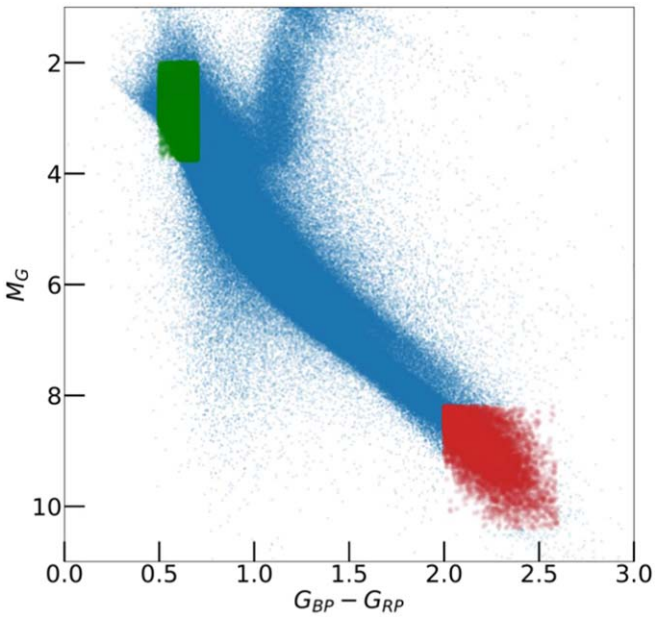

Figure 2. Gaia color–magnitude diagram for 796,757 stars within 300 pc of the Sun. The selected 50,899 high-mass stars and 13,066 low-mass stars are highlighted in green and red, respectively.

For each retained star, we integrate the orbit in the Galactic potential (using the procedure described previously) to determine the star's maximum vertical excursion. For an individual star, $z_{\rm max}$ can be approximated by a random walk process, so that $z_{\rm max} \propto \sqrt{t}$. Knowing that 'Oumuamua has $z_{\rm max} = 27.97$ pc and that Borisov has $z_{\rm max} = 126.46$ pc, the simple diffusion approximation provides an estimate of their ages.

The $z_{\rm max}$ distribution of K- and M-type dwarfs has a long tail toward higher values, providing deviation from a Gaussian distribution. The average $z_{\rm max}$ for the low-mass sample is $\sim$260 pc. This is slightly larger than 210 pc $z_{\rm max}$ for the higher-mass (F-type) stars. The random scattering process follows $z_{\rm max} \propto t^{0.5}$, which has the rate of dispersion flattening with

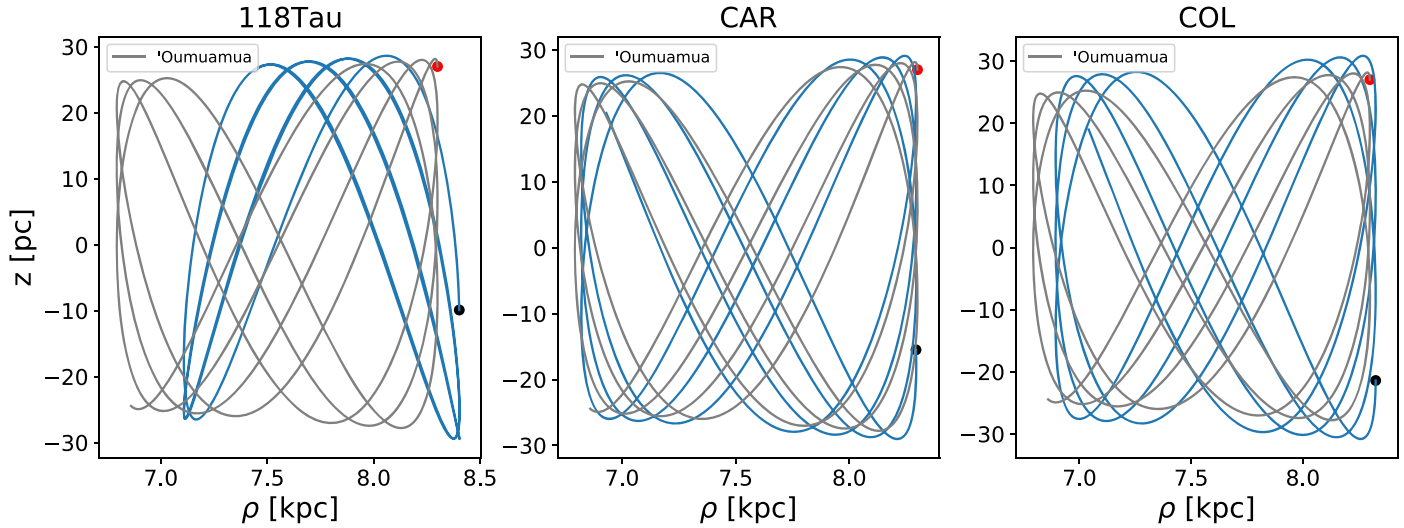

Figure 3. The orbit of 'Oumuamua in the Galactic potential compared to the orbits of three young associations. In each panel, trajectories are propagated 500 Myr into the past in order to facilitate comparison. The quantity ρ charts the distance from the Galactic center. The red and black circles mark the current position of the Sun and the corresponding young association, respectively.

time. The small $z_{\max}$ difference between the low-mass sample and the high-mass sample indicates that $z_{\max}$ is not strongly sensitive to residence times ranging from 2 to $\gtrsim$10 Gyr (the approximate age of the Galactic disk). 'Oumuamua, in particular, has a $z_{\max}$ only 1/10 of the average $z_{\max}$ for the low-mass sample, placing it in the region where $z_{\max}$ is sensitive to age. We note that in general, with the $z_{\max} \propto t^{0.5}$ approach, if we compared 'Oumuamua's $z_{\max}$ to the $z_{\max}$ of higher-mass objects, we would get a more accurate age estimate. We do not use O, B, and A stars on account of their paucity in the solar neighborhood. F-type stars with a Gaussian-like distribution in $z_{\max}$ present the best compromise between youth and abundance.

The F-type stars satisfying criteria 1 and 2 have an average age, $\bar{\tau}_F \sim 2$ Gyr,[4] during which their vertical excursions have evolved to $\bar{z}_F = 210 \pm 160$ pc. We can thus estimate the age $\tau_{\rm ISO}$ of an ISO using $z_{\rm ISO}/\bar{z}_F = \sqrt{\tau_{\rm ISO}/\bar{\tau}_F}$. The vertical excursions of the orbits are obtained from the means of the maximum distances above and below the disk. The maximum vertical excursion of 27.97 pc that we find for 'Oumuamua agrees with the 27.71 pc value calculated by Almeida-Fernandes & Rocha-Pinto (2018; see Almeida-Fernandes & Rocha-Pinto 2018, Table 1 for comparison).[5]

The diffusion model thus gives a $\tau_{\rm 'O} \sim$ 35 Myr age for 'Oumuamua and a $\tau_B \sim 710$ Myr age for Borisov. While rough, this estimate suggests that 'Oumuamua may be significantly younger than 500 Myr. It is thus worthwhile to establish whether it can be connected to known nearby young stellar associations.

Work by Gagné et al. (2018) draws on the Gaia DR1 to identify 27 young stellar associations within 150 pc of the Sun and tabulates the averaged Galactic positions (X, Y, Z) and velocities (U, V, W) for the associations. Using the procedure described above, we integrate these centroids backward in the Galactic potential. The results for the Carina (CAR), Columbia (COL), and 118 Tau moving groups are plotted in Figure 3, and the key properties derived from the simulations of all 27 young stellar associations are shown in Table 1.

Table 1 and Figure 3 show that nearly all of the young associations display maximum vertical excursions that are similar to 'Oumuamua's. The small values for $z_{\max}$ reflect conditions of formation, prior to scattering encounters with molecular clouds and spiral arms. In Table 1 we also list the current normalized radial positions, $(R_0 - R_{\rm min})/\Delta R$. Nearly all of the young associations, like 'Oumuamua, have $R_0 - R_{\rm min}/\Delta R \sim 1$. This indicates that they are all currently near the apocenters of their Galactic orbits, reflecting recent formation (with respect to the ~250 Myr Galactic orbital period) with angular velocities that are less than the local circular velocity.

This phenomenon mainly stems from trapping caused by the gravitational potential perturbation associated with spiral arms and was studied by Roberts & Stewart (1987). Numerical simulations by those authors showed that a spiral arm creates a retrograde relative motion that can entrain the material constituting a given cloud complex for ~50 Myr, a timescale comparable to the lifetime of a molecular cloud. In general, molecular clouds form stars when approaching the minimum of the spiral potential. Therefore, as a consequence of the retrograde motion, one concludes that molecular clouds (with lifetimes <50 Myr) should lie near the apocenters of their Galactic orbits.

Recent simulations by Ramón-Fox & Bonnell (2018) found that gas in the spiral arms can typically have a net radial streaming motion of $v_R \approx -9\,{\rm km\,s^{-1}}$ with an azimuthal velocity deficit of order $6\,{\rm km\,s^{-1}}$ slower than the local circular velocity. This translates to average peculiar motions trending toward the Galactic center and against the sense of Galactic rotation. (Note that the radial oscillation with periodic modulation from spiral arms has a timescale of ~450 Myr; Roberts & Stewart 1987.) We thus expect young associations with ages ≪450 Myr to be near their apocenters and moving with subcircular azimuthal velocities, which is in excellent agreement with the results in Table 1, and to our knowledge,

[4] F-type main-sequence stars have maximum ages of about 4–5 Gyr (Boyajian et al. 2013). For a uniform sampling of F-type stars, a very rough average age should be around $4/2 = 2$ Gyr.

[5] The calculation assumes that the Sun is located at 27 pc above the Galactic plane. 'Oumuamua is at its maximum vertical excursions, and the maximum vertical excursion would be close to the current height of the Sun from the Galactic midplane.

Table 1
Summary of the Simulated Orbits of the 27 Young Stellar Associations within 150 pc

	118 Tau	ABDMG	BPMG	CAR	CARN	CBER	COL	CRA	EPSC	ETAC	HYA	IC 2391	IC 2602	LCC
R_{max}[a]	8.4	8.31	8.3	8.29	8.39	8.43	8.33	8.2	8.26	8.27	8.76	8.34	8.27	8.26
R_{min}[a]	7.11	6.48	7.21	6.82	7.01	7.87	6.89	7.08	6.95	6.77	6.78	7.27	6.85	6.79
z_{max}[a]	29.45	99.4	29.09	29.11	70.46	129.59	30.84	47.79	42.78	71.76	86.75	30.85	94.82	15.76
R_0[a]	8.4	8.31	8.3	8.29	8.3	8.31	8.33	8.17	8.25	8.27	8.34	8.3	8.25	8.25
Z_0[a]	−9.9	−8.8	−15.7	−15.5	−4.3	84.9	−21.4	−42.43	−25.6	−34.81	−15.8	−18.0	−12.6	5.8
$\frac{R_0 - R_{min}}{DR}$	1.0	1.0	1.0	1.0	0.93	0.79	1.0	0.97	0.99	1.0	0.79	0.96	0.99	0.99
Z_0/z_{max}	0.34	0.09	0.54	0.53	0.06	0.66	0.69	0.89	0.6	0.49	0.18	0.58	0.13	0.37
Age[b]	10	149	24	25∼30	200	562	42	4-5	3.7	11	750	50	46	15
Age Ref.	1	2	2	3	4	5	2	6	7	2	8	9	10	11
	OCT	PL8	PLE	ROPH	TAU	THA	THOR	TWA	UCL	UCRA	UMA	USCO	XFOR	
R_{max}[a]	8.3	8.29	8.42	8.2	8.43	8.3	8.39	8.29	8.22	8.19	9.17	8.21	8.33	
R_{min}[a]	8.13	6.75	6.55	7.25	7.8	6.89	7.12	7.08	6.85	6.98	7.77	7.2	6.83	
z_{max}[a]	71.91	53.19	112.81	38.65	42.06	95.87	34.47	32.38	39.04	40.7	49.0	50.16	85.37	
R_0[a]	8.3	8.29	8.42	8.18	8.42	8.29	8.39	8.29	8.19	8.16	8.31	8.18	8.33	
Z_0[a]	−59.7	−13.9	−54.4	37.6	−35.9	−36.1	−23.9	22.7	26.5	−39.2	21.9	48.9	−84.2	
$\frac{R_0 - R_{min}}{DR}$	1.0	1.0	1.0	0.98	0.98	0.99	1.0	1.0	0.98	0.98	0.39	0.97	1.0	
Z_0/z_{max}	0.83	0.26	0.48	0.97	0.85	0.38	0.69	0.7	0.68	0.96	0.45	0.97	0.99	
Age[b]	35	60	112	<2	1–2	45	22	10	16	10	414	10	500	
Age Ref.	12	13	14	15	16	2	2	2	11	17	18	11	19	

Notes.
[a] In units of pc.
[b] In units of Myr.
References. (1) Mamajek 2016; (2) Schneider et al. 2019; (3) Bell et al. 2015; (4) Zuckerman et al. 2006; (5) Silaj & Landstreet 2014; (6) Gennaro et al. 2012; (7) Murphy et al. 2013; (8) Brandt & Huang 2015; (9) Barrado y Navascués et al. 2004; (10) Dobbie et al. 2010; (11) Pecaut & Mamajek 2016; (12) Murphy & Lawson 2015; (13) Platais et al. 1998; (14) Dahm 2015; (15) Wilking et al. 2008; (16) Kenyon & Hartmann 1995; (17) Gagné et al. 2018; (18) Jones et al. 2015; (19) Pöhnl & Paunzen 2010.

this is the first direct observational evidence from Gaia showing that stars form at the apocenter of subcircular orbits.

Among the 27 young associations identified by Gagné et al. (2018), the 30 Myr old group "CAR" (Schneider et al. 2019) and the 42 Myr old group "COL" stand out in terms of their kinematic similarity to 'Oumuamua (Figure 3). Both associations share almost identical maximum vertical excursions and maximum and minimum radial positions with 'Oumuamua and are currently located close to their maximum radial positions from the Galactic center.

If a true physical association exists, we would expect 'Oumuamua's trajectory to intersect the trajectory of the source association at the time of the latter's formation. Moreover, this constraint should be satisfied regardless of whether 'Oumuamua was a comet-like object ejected from a protoplanetary disk or, alternately, a product of the parent GMC itself.

To probe for a physical association, we used the Gala package to explore the range of possible orbits of all 27 young associations. For each association, we integrated 2000 (X, Y, Z, U, V, W) sets drawn from Gaussian distributions in each quantity and conforming to the covariance matrices reported by Gagné et al. (2018). The integrations were all run backward in time for 50 Myr with a time step of 0.1 Myr.

The effect of disk heating on 'Oumuamua's time-reversed trajectory is negligible on a 35 Myr timescale. In the vicinity of the solar neighborhood, the relevant disk heating mechanisms are isotropic heating due to stochastic scattering from molecular clouds and density wave scattering. The density wave mechanism is dominated by the two-arm spiral, which encounters stars twice per orbit (on the timescale of ∼125 Myr). Since the density wave's frequency is close to the local epicyclic frequency, the radial random motion is greatly increased by the near resonance. This would result in the radial velocity dispersion (σ_R) being much greater than vertical velocity dispersion (σ_Z; Jenkins & Binney 1990). Observations have shown that for solar neighborhood stars, $\sigma_Z/\sigma_R \sim 0.5$, suggesting that both spiral density waves and scattering by molecular clouds contribute significantly to the heating of the local disk (Dehnen & Binney 1998; Hänninen & Flynn 2002). Ida et al. (1993) and Sellwood (2008), however, suggest that this anisotropy can be explained by GMC scattering alone. The time-reversed trajectory for a 35 Myr run-out unfolds substantially faster than the timescale for

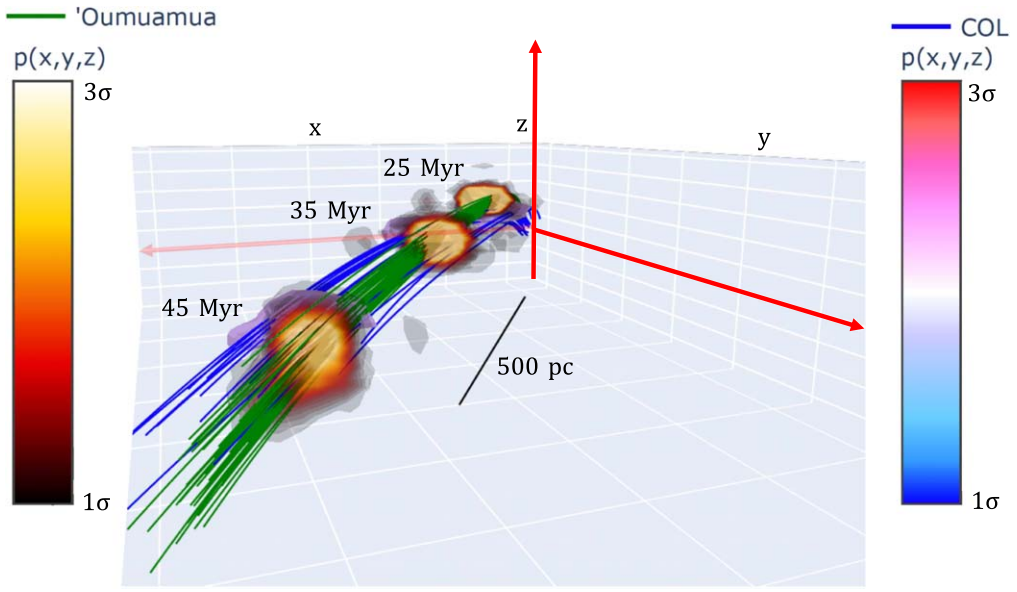

Figure 4. The three-dimensional Galactic orbits of 'Oumuamua and the COL young stellar association integrated backward for 50 Myr. Positive x is in the direction toward the Galactic center. Positive y is in the Galactic rotation direction. Sample trajectories for 'Oumuamua and for stellar members of COL identified by Gagné et al. (2018) are represented by the bundles of green and blue lines, respectively. The colored volumes mark the $1\sigma-3\sigma$ surfaces for both Oumuamua and COL at 25, 35, and 45 Myr. An interactive version of this figure can be found in the online version of the paper.

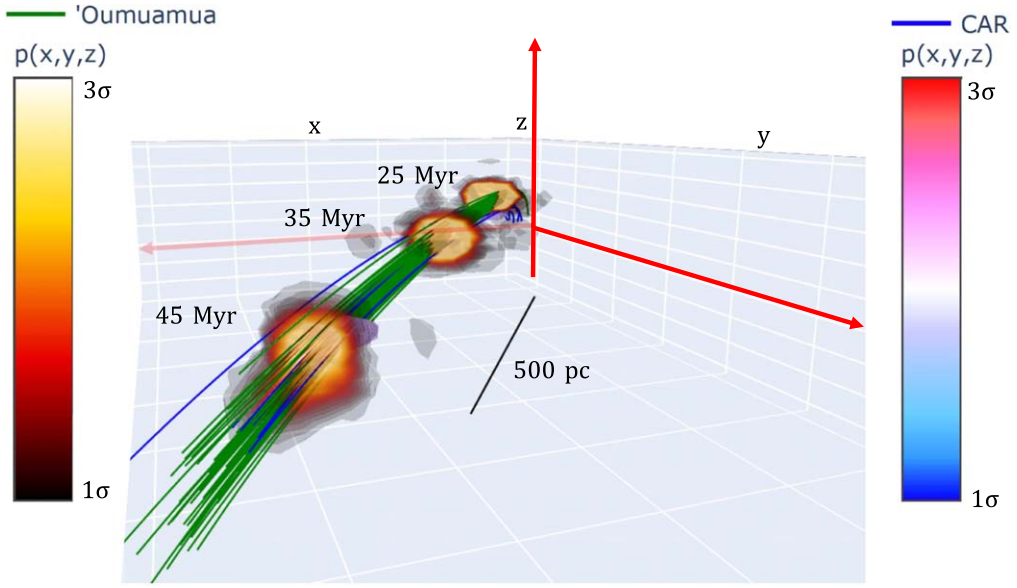

Figure 5. The three-dimensional Galactic orbits of 'Oumuamua and the CAR young stellar association integrated backward for 50 Myr. Positive x is in the direction toward the Galactic center. Positive y is in the Galactic rotation direction. Sampled trajectories for 'Oumuamua and for the stellar members of CAR identified by Gagné et al. (2018) are represented by bundles of green and blue lines, respectively. The colored volumes mark the $1\sigma-3\sigma$ surfaces for both Oumuamua and CAR at 25, 35, and 45 Myr. An interactive version of this figure can be found in the online version of the paper.

spiral-arm heating ($\sim$125 Myr). 'Oumuamua's inferred age is also comparable to the lifetime of a typical molecular cloud, further diminishing the effect of molecular cloud scattering.

The main uncertainty in 'Oumuamua's trajectory stems from the uncertainty in the Sun's Galactic position and velocity. We simulate the allowed range of 'Oumuamua's time-reversed trajectory by perturbing its nominal orbit with 1000 realizations from the Gaussian uncertainty distributions in (X, Y, Z, U, V, W) associated with the Sun's Galactic position and velocity.

In Table 3 of Karim & Mamajek (2017), the authors collected more than 50 estimates of the Sun's height, Z, above the Galactic midplane. We adopted the median value $Z = 17$ pc as the vertical position of the Sun and set the standard deviation to be $\delta z = 10$ pc, which includes almost all the values listed in their table. For the Sun's radial position, X, radial velocity, U, and angular velocity, V, we adopted $X = 8.27 \pm 0.29$ kpc, $U = 13.84 \pm 0.27$ km s^{-1}, and $V = 250 \pm 9$ km s^{-1}, respectively, from Schönrich et al. (2010). For the vertical velocity, W, we adopted the value $W = 7.3$ km s^{-1} used in Aihara et al. (2011). As noted by Schönrich et al. (2010), there is a ~ 4 km s^{-1} systematic difference between the average W motion toward the north and south Galactic poles, possibly indicating a systematic error around ~ 2 km s^{-1}. For simplicity, we adopted $\delta W \sim 2$ km s^{-1} as the standard deviation of the vertical velocity.

The simulated 3D Galactic orbits for CAR, COL, and 'Oumuamua in the solar system's frame are shown in Figures 4 and 5. Interactive versions of these figures are in the online version of the paper. Positive x is in the direction toward the Galactic center. Positive y is in the direction of Galactic rotation. 'Oumuamua's and COL's trajectories are represented by green and blue lines, respectively. The colored volume marks the $1\sigma-3\sigma$ probability surfaces for both 'Oumuamua and COL at 25, 35, and 45 Myr. Note that the dispersions in position for 1000 clones of 'Oumuamua at −50 Myr are (σ_x, σ_y, σ_z) = (18.9, 29.6, 22.2) pc, or $\sigma_r = 41.5$ pc.

Over the past ∼50 Myr CAR and COL have effectively matched orbits with 'Oumuamua. To quantify the degree of intersection between 'Oumuamua and the young associations, we calculate the 1σ intersection volume between 'Oumuamua and the stellar moving groups. The calculation is done by first applying kernel density estimation (KDE) to evaluate the probability of 'Oumuamua and an association at each volume element. Then, three-dimensional 1σ masks enclosing 68% of the probability are calculated to find the intersection. We calculated the 1σ intersection volume for all 27 nearby young stellar associations currently within 150 pc from the Sun between 15 and 50 Myr ago. In total there are only six associations that have nonzero 1σ intersection volumes with 'Oumuamua.

Of these six young associations, only CAR and COL intersect with 'Oumuamua's trajectory at their corresponding ages of 30 and 42 Myr. In particular, the CAR association appears to move in concert with 'Oumuamua and maximizes its 1σ intersection volume with the ISO at around 34 Myr. The 34 Myr peak of CAR's intersection volume is in agreement with the age of ∼25–30 Myr based on the lithium depletion method and its color–magnitude diagram (Schneider et al. 2019). COL, while also intersecting with the ISO, does not maximize its 1σ intersection volume at 42 Myr. This suggests that 'Oumuamua more likely originated from CAR than from COL. It is also important to point out that while the intersection of 3D Galactic orbits favors the origin from CAR, COL cannot be completely ruled out. The intersections with 'Oumuamua at the estimated formation ages, in conjunction with the matching of Galactic orbits, constitute a strong constraint. 'Oumuamua can be counted as a member of Carina or the Columba moving groups. This conclusion echoes the work done by Hallatt & Wiegert (2020), who showed that 'Oumuamua passed through the Carina and Columba moving groups at the time when they were forming.

4. Implications for 'Oumuamua's Origin

By calculating Pan-STARRS's aggregated sensitivity, Do et al. (2018) estimated that the interstellar number density of 'Oumuamua-like objects is of order $n = 0.2\,\mathrm{au}^{-3}$, adopting a cigar or oblate spheroid shape (Belton et al. 2018) with a >6:1 axis ratio (McNeill et al. 2018), effective length smaller than 440 m (Trilling et al. 2018; or effective spherical radius of 102 m), and density of $\sim 3\,\mathrm{g\,cm}^{-3}$, giving a total mass density of $4\,M_\oplus\,\mathrm{pc}^{-3}$. In the previous section, we found support for an origin of 'Oumuamua in the Carina or Columba moving groups. As a consequence, either its detection was a fluke, or we can conclude that similar objects from Carina and Columba suffuse the local interstellar medium.

Figure 6 charts the current positions and velocities of the COL and CAR member stars with respect to the centroids of their respective associations. For 'Oumuamua we plot its ejection velocity from the two young associations and its relative distance from the cluster center. The ejection velocity is estimated by dividing 'Oumuamua's current distance from the cluster center by the cluster age listed in Table 1. We obtain ejection speeds of 1.67 and $0.85\,\mathrm{km\,s}^{-1}$ for CAR and COL, respectively. We note that the current position of 'Oumuamua is closer to the cluster center than the farthest association star for both CAR and COL, which would be expected for a member of either of these associations, and the modest speed is consistent with both the disk ejection and molecular cloud by-product hypotheses (Gaidos et al. 2017; Seligman & Laughlin 2020).

An order-of-magnitude estimate seems to distinguish between the scenarios. Using the Do et al. (2018) estimate of $4\,M_\oplus\,\mathrm{pc}^{-3}$ and spherical volumes defined by the farthest member in the cluster (∼55 pc for CAR, ∼70 pc for COL; see Figure 6), one finds a combined volume for CAR and COL of $\sim 2.1 \times 10^6\,\mathrm{pc}^3$. Naively, this implies an enormous total of $\sim 8.5 \times 10^6\,M_\oplus$ in 'Oumuamua-like objects originating from CAR and COL.

The assigned stellar memberships of CAR and COL vary slightly with the clustering algorithm that is employed, but the associations contain of order 40 stars, implying $2.1 \times 10^5\,M_\oplus$ ejected per star. While crude, this value greatly exceeds the inferred mass of our solar system's planetesimal disk (∼12–65 $M_\oplus$; Nesvorný et al. 2013; Rivera-Valentin et al. 2014; Deienno et al. 2017), suggesting a difficulty with the disk ejection picture (Gaidos et al. 2017).

To refine the foregoing estimate, we conducted a Monte Carlo disk ejection simulation from the seven stars in COL shown in Figure 6. We first back-traced the stars in Figure 6 with time steps of 0.1 Myr and recorded their Galactic positions 30 Myr ago. For each star at this origin moment, we launched 50,000 test particles uniformly over the 4π range of directions with ejection velocities sampled from a Boltzmann-like distribution

$$f\left(x;\frac{1}{\beta}\right) = \frac{1}{\beta}\exp\left(-\frac{x}{\beta}\right), \tag{5}$$

with $\beta = 1\,\mathrm{km\,s}^{-1}$, a speed appropriate to disk ejections by Neptune-like planets. The orbits for each test particle were then integrated 30 Myr forward to the present. We count the number of test particles in a 20 pc box centered at the current position of the Sun to find a number density, $n = 0.006\,\mathrm{pc}^{-3}$. Adjusting for the actual number of stars in CAR, we multiply by (10/7) to get $n \sim 0.0086\,\mathrm{pc}^{-3}$. In order to match the Do et al. (2018) estimate of $\sim 0.2\,\mathrm{au}^{-3}$, of order $\sim 1 \times 10^{21}$ 'Oumuamua-like objects must be ejected from each star. Adopting a mass $M \sim 10^9$ kg for 'Oumuamua (Do et al. 2018), this corresponds to $1.7 \times 10^5\,M_\oplus$ or $\sim 540\,M_{\mathrm{Jup}}$, a value in line with the simpler estimate given above.

A large number density is better understood if 'Oumuamua's origin can be attributed to a formation process that is endemic to a molecular cloud core and that does not involve protostellar disks. A possible mechanism involving molecular hydrogen ice has been outlined by Seligman & Laughlin (2020) and is explored in depth by Levine & Laughlin (2021), who conclude that H_2 ice deposition in molecular cloud cores is very difficult but perhaps not impossible to achieve. Alternately, Desch & Jackson (2021) proposed that 'Oumuamua is a nitrogen ice fragment produced by impacts onto Pluto-like nitrogen-

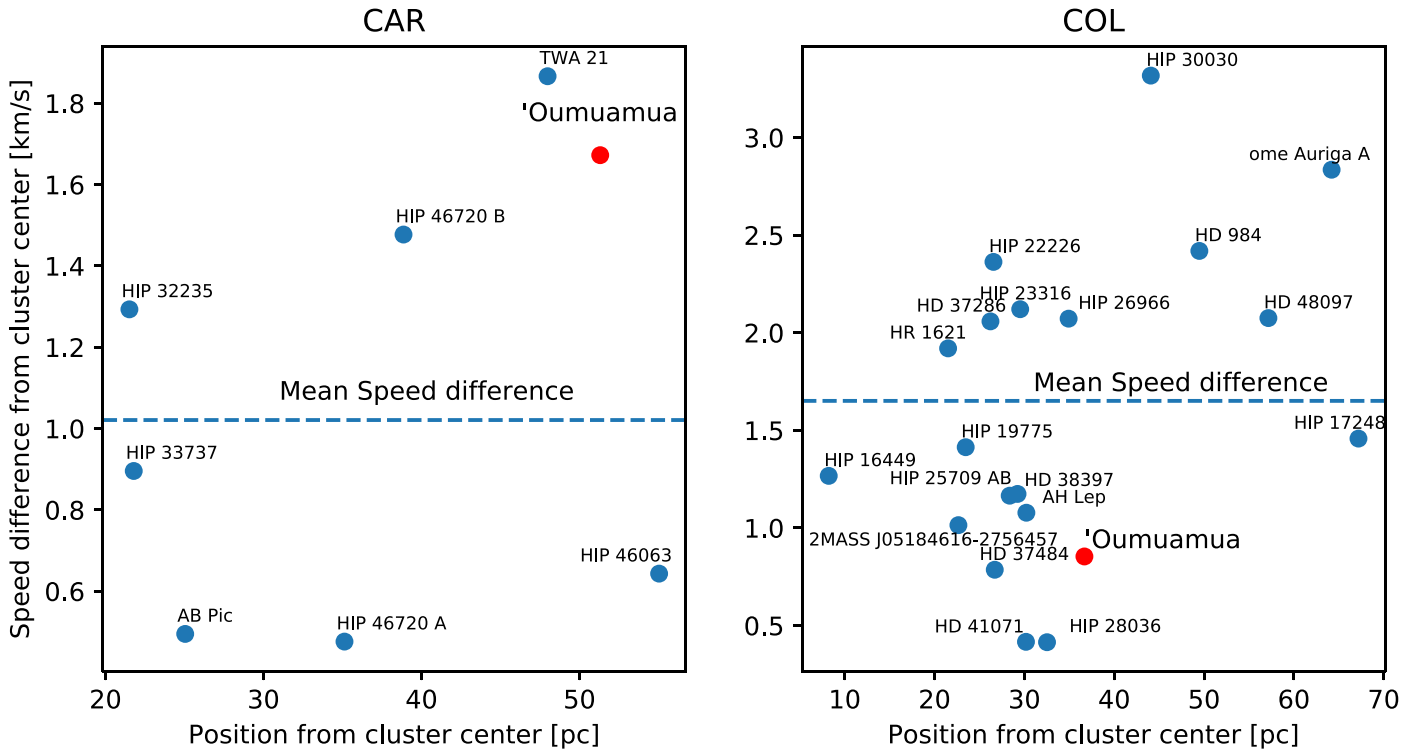

Figure 6. The distributions of COL and CAR member stars in position and velocity space relative to the cluster centers. Note that for 'Oumuamua the ejection velocity is plotted on the *y*-axis instead of the speed difference from the cluster center.

surfaced objects in exoplanetary systems. This hypothesis satisfies the dynamical and photometric constraints but requires a very high rate of such collisions.

In any event, we have shown that 'Oumuamua's Galactic orbit is strongly suggestive of an origin in the COL or CAR moving group. Yet intriguingly, the large resulting inferred number density is in strong conflict with a disk product hypothesis for its origin and is in significant tension with a cloud product hypothesis. Resolution of the mystery will very likely require observation of additional 'Oumuamua-like objects.

This material is based on work supported by the National Aeronautics and Space Administration through the NASA Astrobiology Institute under Cooperative Agreement Notice NNH13ZDA017C issued through the Science Mission Directorate. We acknowledge support from the NASA Astrobiology Institute through a cooperative agreement between NASA Ames Research Center and Yale University. The authors further thank Darryl Seligman and Sam Cabot for informative discussion on interstellar objects.

Software: Rebound, Astropy (The Astropy Collaboration 2013, 2018).

ORCID iDs

Cheng-Han Hsieh https://orcid.org/0000-0003-2803-6358
Gregory Laughlin https://orcid.org/0000-0002-3253-2621
Héctor G. Arce https://orcid.org/0000-0001-5653-7817

References

Aihara, H., Allende Prieto, C., An, D., et al. 2011, ApJS, 195, 26
Almeida-Fernandes, F., & Rocha-Pinto, H. J. 2018, MNRAS, 480, 4903
Bannister, M. T., Schwamb, M. E., Fraser, W. C., et al. 2017, ApJL, 851, L38
Barrado y Navascués, D., Stauffer, J. R., & Jayawardhana, R. 2004, ApJ, 614, 386
Bell, C. P. M., Mamajek, E. E., & Naylor, T. 2015, MNRAS, 454, 593
Belton, M. J. S., Hainaut, O. R., Meech, K. J., et al. 2018, ApJL, 856, L21
Bolin, B. T., Lisse, C. M., Kasliwal, M. M., et al. 2020, AJ, 160, 26
Bolin, B. T., Weaver, H. A., Fernandez, Y. R., et al. 2018, ApJL, 852, L2
Bovy, J. 2015, ApJS, 216, 29
Boyajian, T. S., von Braun, K., van Belle, G., et al. 2013, ApJ, 771, 40
Brandt, T. D., & Huang, C. X. 2015, ApJ, 807, 24
Dahm, S. E. 2015, ApJ, 813, 108
Dehnen, W., & Binney, J. J. 1998, MNRAS, 298, 387
Deienno, R., Morbidelli, A., Gomes, R. S., et al. 2017, AJ, 153, 153
Desch, S. J., & Jackson, A. P. 2021, JGR, 126, e06807
Do, A., Tucker, M. A., & Tonry, J. 2018, ApJL, 855, L10
Dobbie, P. D., Lodieu, N., & Sharp, R. G. 2010, MNRAS, 409, 1002
Domokos, G., Sipos, A. Á., Szabó, G. M., et al. 2017, RNAAS, 1, 50
Dormand, J. R., & Prince, P. J. 1980, JCoAM, 6, 19
Füglistaler, A., & Pfenniger, D. 2018, A&A, 613, A64
Gagné, J., Mamajek, E. E., Malo, L., et al. 2018, ApJ, 856, 23
Gaia Collaboration, Brown, A. G. A., Vallenari, A., et al. 2018, A&A, 616, A1
Gaidos, E., Williams, J., & Kraus, A. 2017, RNAAS, 1, 13
Gennaro, M., Prada Moroni, P. G., & Tognelli, E. 2012, MNRAS, 420, 986
Hallatt, T., & Wiegert, P. 2020, AJ, 159, 147
Hänninen, J., & Flynn, C. 2002, MNRAS, 337, 731
Hernquist, L. 1990, ApJ, 356, 359
Hoang, T., & Loeb, A. 2020, ApJL, 899, L23
Ida, S., Kokubo, E., & Makino, J. 1993, MNRAS, 263, 875
Jenkins, A., & Binney, J. 1990, MNRAS, 245, 305
Jewitt, D., Luu, J., Rajagopal, J., et al. 2017, ApJL, 850, L36
Jones, J., White, R. J., Boyajian, T. S., et al. 2015, AAS Meeting Abstracts, 225, 112.03
Karim, M. T., & Mamajek, E. E. 2017, MNRAS, 465, 472
Kent, S. M., Dame, T. M., & Fazio, G. 1991, ApJ, 378, 131
Kenyon, S. J., & Hartmann, L. 1995, ApJS, 101, 117
Knight, M. M., Protopapa, S., Kelley, M. S. P., et al. 2017, ApJL, 851, L31
Levine, W. G., & Laughlin, G. 2021, ApJ, 912, 3
Levison, H. F., Morbidelli, A., Van Laerhoven, C., et al. 2008, Icar, 196, 258
López-Corredoira, M., Cabrera-Lavers, A., Garzón, F., et al. 2002, A&A, 394, 883
Mamajek, E. E. 2016, in Proc. IAU Symp. 314, Young Stars & Planets Near the Sun (Cambridge: Cambridge Univ. Press), 21

Mamajek, E. 2017, RNAAS, 1, 21
Mashchenko, S. 2019, MNRAS, 489, 3003
McMillan, P. J. 2011, MNRAS, 414, 2446
McNeill, A., Trilling, D. E., & Mommert, M. 2018, ApJL, 857, L1
Meech, K. J., Weryk, R., Micheli, M., et al. 2017, Natur, 552, 378
Micheli, M., Farnocchia, D., Meech, K. J., et al. 2018, Natur, 559, 223
Miyamoto, M., & Nagai, R. 1975, PASJ, 27, 533
Murphy, S. J., & Lawson, W. A. 2015, MNRAS, 447, 1267
Murphy, S. J., Lawson, W. A., & Bessell, M. S. 2013, MNRAS, 435, 1325
Navarro, J. F., Frenk, C. S., & White, S. D. M. 1997, ApJ, 490, 493
Nesvorný, D., Vokrouhlický, D., & Morbidelli, A. 2013, ApJ, 768, 45
Nordström, B., Mayor, M., Andersen, J., et al. 2004, A&A, 418, 989
Pecaut, M. J., & Mamajek, E. E. 2016, MNRAS, 461, 794
Platais, I., Kozhurina-Platais, V., & van Leeuwen, F. 1998, AJ, 116, 2423
Pöhnl, H., & Paunzen, E. 2010, A&A, 514, A81
Price-Whelan, A. M. 2017, JOSS, 2, 388
Ramón-Fox, F. G., & Bonnell, I. A. 2018, MNRAS, 474, 2028
Rein, H., & Liu, S.-F. 2012, A&A, 537, A128
Rein, H., & Spiegel, D. S. 2015, MNRAS, 446, 1424
Rivera-Valentin, E. G., Barr, A. C., Lopez Garcia, E. J., et al. 2014, ApJ, 792, 127
Roberts, W. W., & Stewart, G. R. 1987, ApJ, 314, 10
Schneider, A. C., Shkolnik, E. L., Allers, K. N., et al. 2019, AJ, 157, 234
Schönrich, R., Binney, J., & Dehnen, W. 2010, MNRAS, 403, 1829
Sekanina, Z. 2019, arXiv:1905.00935
Seligman, D., & Laughlin, G. 2020, ApJL, 896, L8
Sellwood, J. A. 2008, in ASP Conf. Ser. 396, Formation and Evolution of Galaxy Disks (San Francisco, CA: ASP), 341
Silaj, J., & Landstreet, J. D. 2014, A&A, 566, A132
Trilling, D. E., Mommert, M., Hora, J. L., et al. 2018, AJ, 156, 261
Tsiganis, K., Gomes, R., Morbidelli, A., et al. 2005, Natur, 435, 459
White, R. S. 1996, Ap&SS, 240, 75
Wilking, B. A., Gagné, M., & Allen, L. E. 2008, in Handbook of Star Forming Regions, ed. B. Reipburth, Vol. 2 (San Francisco, CA: ASP), 351
Zuckerman, B., Bessell, M. S., Song, I., et al. 2006, ApJL, 649, L115